ACS Sustainable Chemistry & Engineering

pubs.acs.org/journal/ascecg

Research Article

Cellulosic Ternary Nanocomposite for Affordable and Sustainable Fluoride Removal

Moses Egor,[‖] Avula Anil Kumar,[‖] Tripti Ahuja, Sritama Mukherjee, Amrita Chakraborty, Chennu Sudhakar, Pillalamarri Srikrishnarka, Sandeep Bose, Swathy Jakka Ravindran, and Thalappil Pradeep*

Cite This: *ACS Sustainable Chem. Eng.* 2021, 9, 12788−12799

Read Online

ACCESS | Metrics & More | Article Recommendations | Supporting Information

ABSTRACT: Adsorption is shown to be an extremely affordable and sustainable way of producing clean water, particularly in resource-limited settings. In this paper, we sought to synthesize an effective cellulose-based composite adsorbent from eco-friendly, earth-abundant, and consequently affordable ingredients at room temperature for fluoride removal from drinking water. We utilized the synergistic effect of various renewable materials and active sites of metal oxyhydroxides in developing an effective adsorbent, which is physically stable under the conditions of use. Nanoscale oxyhydroxides of aluminum and iron were scaffolded into a matrix of carboxymethyl cellulose (CMC) to form a nanocomposite adsorbent, which was prepared in water, eventually making a water-stable porous solid. This was used in batch and cartridge adsorption experiments for fluoride removal. The adsorbent surface before (*in situ*) and after fluoride uptake was characterized using various analytical techniques. The *in situ* composite exhibited a surface area of 134.3 m^2/g with an amorphous solid structure with Al and Fe uniformly distributed in the cellulose matrix. From the batch adsorption experiments, we observed 80% fluoride removal within the first 3 min of contact, with a maximum uptake capacity of 75.2 mg/g as modeled by the Langmuir adsorption isotherm, better than most reported materials. The adsorbent effectively reduced F^- levels in field water from 10 to 0.3 mg/L, less than 1.5 mg/L the World Health Organization upper limit for drinking water. Optimum F^- removal was achieved between the pH of 4−9; however, the effectiveness of the adsorbent was reduced in the presence of competing ions in the order $PO_4^{3-} > SiO_3^{2-} > CO_3^{2-} > HCO_3^- > SO_4^{2-}$. A cartridge experiment demonstrated the applicability of the adsorbent in a domestic point-of-use water purifier for defluoridation. Sustainability metrics of the material were evaluated. Defluoridation using the material is estimated to cost $3.3 per 1000 L of treated water at the scale of community implementation projects.

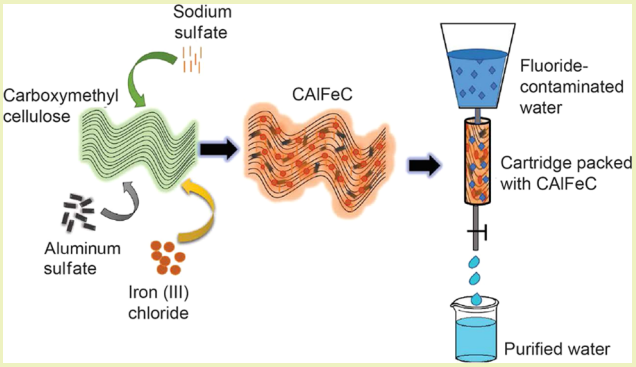

KEYWORDS: *fluoride, defluoridation, carboxymethyl cellulose, iron oxyhydroxide, aluminum oxyhydroxide, composite adsorbent*

INTRODUCTION

Adsorption is widely used in environmental remediation applications, including air and water purification, targeting a wide range of organic and inorganic pollutants. Many water purification technologies utilize a variety of inorganic adsorbents such as oxides of Al, Fe, Ca, and Mn, silicates, and carbon-based adsorbents.[1−4] Biosorbents synthesized from alginates, chitosan, cellulose, and their derivatives with various functionalities have also been successfully applied in water purification.[5,6] On their own, these materials may not be very effective adsorbents and are often unstable and hence disintegrate in water, causing further contamination.[7] Efforts have been made to scaffold metal oxides in polymer frameworks for synergistic enhancement of adsorption capacity, along with stability.[8−10] Composite adsorbents consisting of metal oxyhydroxides embedded in organic polymer matrices have gained the attention of researchers due to their high adsorption efficiency and stability in aqueous media.[11−13] Such adsorbents utilizing organic matrices of chitosan, alginate, and cellulose, in which nanoparticles of metal oxides and hydroxides are confined, have been widely used to remove arsenic, Cr^{6+}, dyes, and fluoride from water.[5,11,14,15] Wang, Lin, Luo, and Long loaded Zr^{4+} onto carboxymethyl cellulose and reported impressive fluoride removal capacity of up to 47 mg/g. These and other studies[15−17] highlight the effectiveness of composite adsorbent

Received: May 15, 2021
Published: September 14, 2021

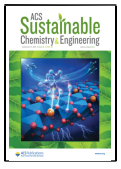

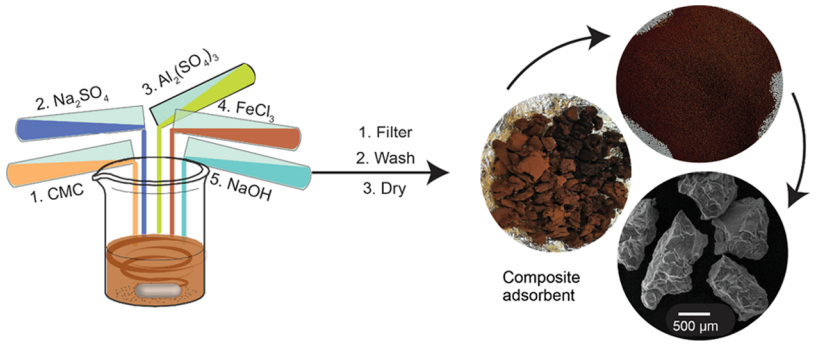

Figure 1. Schematic diagram illustrating the synthesis of CAlFeC.

materials used in the sequestration of both cationic and anionic water pollutants.

Over 30 countries are grappling with the health problems related to the ingestion of excess F^- (>1.5 mg/L) in surface and groundwater sources.[18] Fluorosis is prevalent in China, India, South America, North Africa, and countries along the East African rift valley. Fluoride pollution, therefore, is a global problem spanning nearly all geographical locations.[19] It is therefore evident that the need to develop affordable, effective, environmentally friendly, and sustainable defluoridation technologies can only increase, given the current and projected global demand for clean water. A key aspect of providing new solutions is affordability, implying the use of earth-abundant materials and simple processing.

In this paper, we present the facile synthesis, characterization, and application of a cellulose-based adsorbent referred to as a cellulose-Al-Fe nanocomposite (abbreviated as CAlFeC) by incorporating AlOOH and FeOOH into a carboxymethyl cellulose (CMC) matrix, which was used as an effective adsorbent to remove excess fluoride from water to bring it down to below the permissible guideline (<1.5 mg/L) of WHO. These metal oxyhydroxides have been shown to bear high adsorption potential owing to their metastable state, higher surface area due to their porous structures, nanoscale confinement in the polymer cages, and exposure of active surfaces for adsorption. CMC provides a rigid cellulose backbone onto which the metal oxyhydroxides are embedded, providing strength and rigidity even after prolonged exposure to water. Aluminum compounds have been shown to have very good F^- uptake capacity in several studies,[4,19] while iron(III) oxides provide structural rigidity and strength when embedded in polymer cages. Another similar study suggests that the synergistic action of these three main components is known to offer a rigid material with good adsorption capacity.[13] CAlFeC was used in batch and cartridge adsorption experiments to investigate adsorption kinetics in simulated field applications. The adsorbent was characterized before and after fluoride uptake using standard analytical techniques and a possible mechanism of F^- adsorption was developed.

From our evaluation, CAlFeC is a stable and effective adsorbent for fluoride, applicable under a wide range of environmental water conditions. At the adsorbent dose of 1 g/L, CAlFeC can be used to effectively reduce fluoride levels from 20 to <1.5 mg/L. From Table 2, even at elevated fluoride levels >20 mg/L, the amount of fluoride removed (q_e) increased, and increasing the adsorbent dose can achieve the desired 1.5 mg/L limit in the treated water. The material is easily synthesized from readily available nontoxic reagents and water as the only solvent used. All reactions were conducted at room temperature and under ordinary laboratory conditions without the need for sophisticated equipment or specialized skills. The ease and greenness of synthesis and the properties highlighted make CAlFeC suitable for use in low-income settings.

EXPERIMENTAL SECTION

Materials. Carboxymethyl cellulose (CMC) was purchased from Avantor Performance Materials India Ltd. Aluminum sulfate octadecahydrate ($Al_2(SO_4)_3{\cdot}18H_2O$) was purchased from Loba Chemie Pvt. Ltd., India. Ferric chloride hexahydrate ($FeCl_3{\cdot}6H_2O$) and NaOH were purchased from RANKEM Glassware and Chemicals Pvt. Ltd., India. Sodium sulfate anhydrous (Na_2SO_4) and sodium fluoride (NaF) were purchased from Merck India Ltd. All chemicals were of high-purity analytical grade and were used without further purification. Distilled water (DW) was used in all synthetic processes. Ultrapure water (QW) of electrical conductivity ~0.05 μS/cm and tap water (TW) of about 800 μS/cm were used in some batch adsorption experiments as described. Fluoride was determined by the ion-selective electrode (ISE) method (Thermo Scientific, Orion BNWP 96009). All reactions were carried out in polypropylene labware.

Methods: Synthesis of CAlFeC. About 132 mg of CMC, a cellulose precursor, was dissolved in 10 mL of DW and ultrasonicated for 5 min, followed by the addition of 1.4 g of sodium sulfate anhydrous with constant stirring for 1 h until the salt was dissolved. To this, 0.5 M aluminum sulfate solution (4 mL) was added, and the mixture was incubated for 3 h, followed by the addition of 1 M ferric chloride hexahydrate solution (4 mL), and was further incubated for 1 h. Sodium hydroxide solution (2 M) was added (about 15 mL) dropwise to adjust the pH of the mixture to 7. The resultant brown gel was further incubated for 12 h with vigorous stirring at room temperature, after which it was filtered and washed thoroughly with distilled water until the conductivity of the washed water was ≤200 μS/cm. The composite material formed was oven-dried at 60 °C for 12 h, after which it was ground, sieved to desired particle sizes, and used in fluoride adsorption studies. Figure 1 below shows a summary of the procedure used to synthesize CAlFeC.

The optimized synthetic protocol of CAlFeC above was arrived at after several separate reactions in which different parameters were optimized. The effect of polyvalent cations (Ca^{2+}, Mg^{2+}, Mn^{2+}, Zn^{2+}, Ce^{3+}, La^{3+}, Zr^{3+}, Ti^{4+}) and anions (SO_4^{2-}, SiO_3^{2-}, PO_4^{3-}, CO_3^{2-}, HCO_3^-) on the adsorbent structure was investigated. Each time, dry lumps of the solid adsorbent were shaken at 200 rpm with distilled water to evaluate the stability under wet conditions. The experimental conditions that yielded the adsorbent with the best balance of fluoride uptake and physical hardness (tested both in dry and wet conditions) were chosen for bulk synthesis and batch adsorption experiments. The adsorbent was ground and sieved to obtain particle sizes of 300, 212, and <150 μm (referred to as powder).

Adsorption Experiments. Effects of particle size, adsorbent dose, contact time, pH, initial adsorbate (fluoride) concentration, co-ions usually present in water, and the number of reusable cycles were evaluated in batch experiments. The aforementioned variables were

https://doi.org/10.1021/acssuschemeng.1c03272
ACS Sustainable Chem. Eng. 2021, 9, 12788−12799

Table 1. Synergistic Effect of Components on the Strength and Effectiveness of CAlFeC

	composition				strength of material			
sample ID	CMC	Na_2SO_4	$Al_2(SO_4)_3$	$FeCl_3$	dry	wet	color of treated water	fluoride uptake (%)
CAlFeC1	√	√	√	—	very poor	very poor	turbid	95
CAlFeC2	√	√	—	√	excellent	excellent	very clear	24
CAlFeC3	√	—	√	√	poor	very poor	brown	96
CAlFeC4	—	√	√	√	poor	very poor	turbid	94
CAlFeC5	√	√	√	√	very good	very good	very clear	97

optimized to obtain the best conditions for the subsequent batch experiments. Typically, 100 mg of CAlFeC was placed in contact with 100 mL of 10 mg/L fluoride solution separately in DW and TW in a 250 mL polypropylene Erlenmeyer flask and shaken at 200 rpm in an orbital shaker for 2 h. The adsorption capacity of the material at particle sizes of 300 and 212 μm and powder was tested separately. After shaking, the mixture was decanted, and residual fluoride in the supernatant was determined by the ISE method (US-EPA method 9214). Fluoride-spiked laboratory TW was used to mimic environmental water. The choice of particle sizes of 300 and 212 μm was due to their applicability in cartridge packing in realistic applications.

The regeneration ability of CAlFeC was investigated using 0.1, 1, and 2 mol/L NaOH solutions as eluents. For the first cycle, a freshly prepared 10.3 mg/L fluoride-spiked water was placed in contact with CAlFeC for approximately 12 h. For the next cycle, the used adsorbent was filtered off and washed several times with NaOH solution and rinsed with DW, and then oven-dried at 60 °C.

Characterization of the Adsorbent. Fourier transform infrared spectroscopy (FTIR), Raman spectroscopy, X-ray diffractometry (XRD), scanning electron microscopy-energy-dispersive X-ray spectrometry (SEM-EDS), high-resolution transmission electron microscopy-energy-dispersive X-ray spectrometry (HRTEM-EDS), and Brunauer–Emmett–Teller (BET) surface area analysis techniques were used to characterize the adsorbent before and after fluoride uptake. SEM imaging was done with an FEI Quanta 200 coupled to the EDS system. Powdered samples of CAlFeC and fluoride-loaded CAlFeC (CAlFeC-F) were spread on carbon strips, sputter-coated with gold, and mounted. Powder XRD patterns of CAlFeC and CAlFeC-F were determined using a Bruker D8 Advance spectrometer at the Department of Chemistry, Indian Institute of Technology Madras, India. Raman spectra of CMC, CAlFeC, and CAlFeC-F were recorded using a confocal Raman spectrometer with 633 nm as the excitation source. BET surface area was measured by nitrogen adsorption–desorption experiments using a BET surface area analyzer (Micromeritics ASAP 2020). XPS analyses of elemental compositions of CAlFeC before and after its interaction with fluoride were performed using an ESCA Probe TPD spectrometer, Omicron Nanotechnology. Direct shear stress measurements were performed to determine the physical strength of the material in dry and wet conditions. The leaching of metals (Al and Fe) and total organic carbon (TOC) into the treated water was evaluated using the US-EPA method 1311. PerkinElmer NexION 300X inductively coupled plasma mass spectrometry (ICPMS) with appropriate standards and a TOC analyzer, Shimadzu TOC-V_{CPH}, were used to determine metal concentrations and TOC, respectively.

RESULTS AND DISCUSSION

Effect of Incorporating Other Polyatomic Anions as Binders. A crucial aspect of the material is its stability in water. We observed that sodium sulfate is essential for the stability and physical hardness of the material. Without it, the solid formed was easily crushed into powder, which would not be desirable in a water filtration column or cartridge as this would cause a pressure drop and possible leaching of its constituents into the treated water. Sulfate ions provide a stable linkage between cellulose fibers and the metal oxyhydroxides. In Figure 5, we have suggested a possible mechanism of binding of sulfate to facilitate crosslinking between cellulose chains, utilizing the OH groups.[21] The presence or absence of sodium sulfate, however, did not affect the fluoride uptake capacity of the adsorbent. It is known that carbonate and bicarbonate ions in solution interfere most with fluoride adsorption.[22] However, when carbonate and bicarbonate, instead of sulfate, were incorporated as binders into the adsorbent solid structure, there was a slight improvement in fluoride adsorption. The resulting adsorbent was, however, too soft to make a good filter cartridge or column packing. When sulfate was substituted with phosphate and silicate anions as stabilizers, there was a drastic reduction in the fluoride removal efficiency of the adsorbent (Figure S1B). The composite in which phosphate anion was incorporated as a binder formed a thick gel that could not be filtered or washed, and therefore its bulk synthesis was not viable. The addition of sodium sulfate, therefore, gave the best balance between fluoride removal, physical hardness of the solid adsorbent, and ease of gel separation. Poor fluoride uptake observed due to phosphate and silicate is attributed to their interference with adsorption sites and low porosity of the resultant adsorbent. This is consistent with a report of Kumar et al.[11]

Effect of Incorporating Other Polyvalent Cations. We investigated the effect of adding different polyvalent cations (Ca^{2+}, Mg^{2+}, Mn^{2+}, Zn^{2+}, Ce^{3+}, La^{3+}, Zr^{3+}, and Ti^{4+}) on the strength and fluoride uptake capacity of CAlFeC. The addition of other polyvalent cations gave mixed results, with some cations (Mg^{2+}, Mn^{2+}, and Zn^{2+}) resulting in better strength of the material but with very low fluoride uptake (Figure S1A), while others (Ca^{2+}, Ce^{3+}, La^{3+}, Zr^{3+}, and Ti^{4+}) resulted in a slight improvement in fluoride uptake performance with poor strength. However, the improvement was not significant enough to justify the additional cost of incorporating these extra components. It was observed that excluding Al^{3+} from the composition of the adsorbent drastically reduced its ability to remove fluoride, while the elimination of CMC, sodium sulfate, and ferric chloride yielded a very soft solid that completely disintegrated in water. The optimized composition described, therefore, yielded just the correct ratio of CMC/Al/Fe for the best balance of green strength, fluoride removal, and ease of gel separation. Fluoride removal capacity was lower in TW compared to DW due to the presence of competing ions. Figure S1A,B in the Supporting Information (SI) shows an increase in fluoride uptake capacity as the adsorbent particle size was reduced (from 300 μm to powder). A high surface area of powdered solid exposed more adsorption sites and hence improved the efficiency. However, granular solids (micron particles) are preferred for cartridge packing than powder to enhance hydraulic conductivity.

Synergistic Effect of the Components of CAlFeC. From the experiments done to investigate the effect of adding or removing the different components of CAlFeC, we found a cooperative interaction of the components to enhance the

https://doi.org/10.1021/acssuschemeng.1c03272
ACS Sustainable Chem. Eng. 2021, 9, 12788–12799

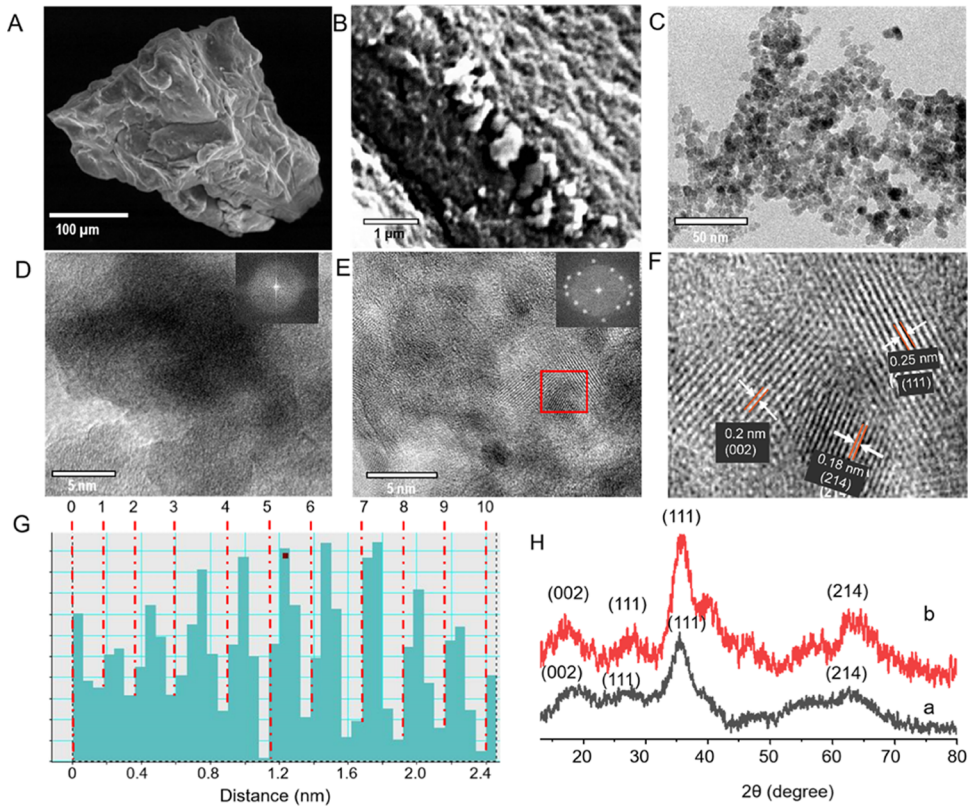

Figure 2. Micrographs and crystallographic features of CAlFeC showing SEM images (A, B; at a micron scale). HRTEM images (C–E) before beam irradiation (D) and after beam irradiation (E) with insets of corresponding FFT images. (F) Enlarged section of (E) showing lattice-resolved planes. (G) Lattice distance profile of FeOOH nanoparticles for the (111) crystal plane. It is a profile of 10 consecutive lattice planes, an average of which was considered as the lattice distance between the planes. (H) Powder X-ray diffraction patterns of CAlFeC before (a) and after (b) fluoride uptake.

properties of the adsorbent, i.e., its strength and effectiveness. As can be seen in Table 1, removing one or more of the components negatively affected the adsorption effectiveness and physical strength of the material. The increase in strength is attributed to entropic stabilization as more components are added, a phenomenon encountered in high entropy alloys. Fe^{3+} and Al^{3+}, upon interaction with other components of CAlFeC, and during coprecipitation with NaOH, resulted in the formation of a stable multicomponent system of different oxides, oxyhydroxides, and hydroxides, as confirmed by PXRD analysis. We determined that Al^{3+}, being a harder acid than Fe^{3+}, accounts for most of the fluoride removal capacity, while CMC, sulfate, and Fe^{3+} are mainly responsible for the structural rigidity of CAlFeC.

SEM images revealed a layered structure after the saturation of the composite surface with fluoride ions (Figure 2B). Elemental maps and EDS spectra show a fluoride signal only after fluoride adsorption (Figure S3). This confirms that fluoride is adsorbed and uniformly distributed on the adsorbent surface, as can be confirmed from mapping images in Figure S3A compared to S3B. HRTEM-EDS imaging of the adsorbent was carried out using a JEM 3010 (JEOL, Japan) coupled to the Oxford Semistem EDS system. The samples for HRTEM were prepared as drop-casts of the dispersion on carbon films supported on a copper grid and dried. Figure 2C–F shows the high-resolution transmission electron microscopic (HRTEM) images of CAlFeC at different magnifications. Figure 2D,E shows the time-dependent images of the same frame with insets of respective fast Fourier transform (FFT) images. The electron beam irradiation induced crystallization of the adsorbent structure. This is attributed to the crystallization of iron oxide/oxyhydroxide/hydroxide, which usually changes to more crystalline phases by electron irradiation.[23] Figure S4 presents the HRTEM elemental maps and atomic percentages of CAlFeC and CAlFeC-F, confirming fluoride uptake.

Lattice-resolved HRTEM image of CAlFeC (Figure 2F) reveals clear crystal planes (002), (111), and (214) with interplanar distances of 0.2, 0.245, and 0.18 nm of FeOOH, respectively. Semicrystalline nanoparticles of goethite and pseudoboehmite are responsible for the crystalline phases embedded in a largely amorphous cellulose matrix. The observed crystallization is due to the electron beam irradiation of the material. This results in more stable oxides/oxyhydroxides of Fe and Al such as hematite, goethite, and gibbsite by electron beam-induced crystallization.[13] This is corroborated by powder X-ray diffraction (PXRD) patterns of CAlFeC and CAlFeC-F.

In Figure 2H, the PXRD patterns reveal a largely amorphous solid structure with a few broad and less-intense peaks at 36 and 63° corresponding goethite (α-FeOOH) JCPDS no. 29-713. Other less-intense peaks that appeared at 27 and 57° matched with boehmite (γ-AlOOH), based on JCPDS no. 21-1307.[8] These crystalline phases also matched with the inorganic crystal structure database (ICSD) of goethite (α-FeOOH), gibbsite, hematite, hydrohematite, and a mixed Fe/Al oxyhydroxide with ICSD reference codes 03-0251, 33-0018, 89-8103, 33-664, and 13-157, respectively, from the ICSD

https://doi.org/10.1021/acssuschemeng.1c03272
ACS Sustainable Chem. Eng. 2021, 9, 12788–12799

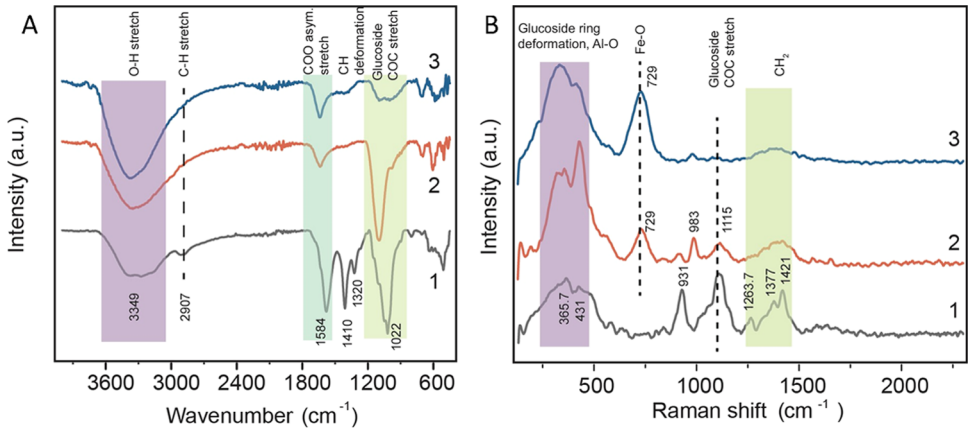

Figure 3. Vibrational spectroscopic features of the materials. (A) FTIR spectra of CMC (1), CAlFeC (2), and CAlFeC-F (3). (B) Raman spectra of CMC (1), CAlFeC (2), and CAlFeC-F (3). Note that FTIR data are presented in the transmission mode, and Raman data are in terms of scattering intensity.

database.[24,25] This confirms the presence of a mixture of metastable oxyhydroxides and oxides of iron and aluminum in the adsorbent structure. The high surface energies of these phases are responsible for the high adsorption capacity. Other previous studies[25,26] have shown that the FeOOH and AlOOH can be transformed to more crystalline phases by electron beam irradiation in TEM.

FTIR spectra of CMC, CAlFeC, and CAlFeC-F are presented in Figure 3A. The broad peak between 3200 and 3400 cm^{-1} is attributed to the stretching modes of O−H vibrations. This peak is more intense in CAlFeC and CAlFeC-F, which is due to the additional OH groups from metal oxyhydroxides and interstitial water molecules. Displacement of sodium ions and subsequent protonation of the carboxylate groups of CMC is another plausible explanation for the amplification of this feature. The peak at 2907 cm^{-1} corresponds to the −C−H stretching vibrations. This peak disappeared in CAlFeC and CAlFeC-F. The disappearance of $-CH_2-$ features is also seen at 1410 and 1320 cm^{-1}, an indication of strong binding of cellulose chains with metal oxyhydroxides during synthesis.

From Figure 3A, the peak at 1584 cm^{-1} is attributed to the asymmetric stretching of COO^- groups,[27] which diminished in CAlFeC and CAlFeC-F and shifted to 1640 cm^{-1}. This is due to the direct coordination of the carboxylate group to metal ions in a bidentate fashion, as indicated below.[28]

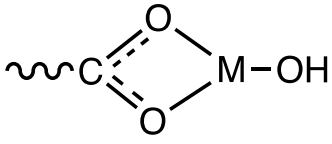

This confirms the participation of the COO^- group in strong metal binding during the formation of the nanocomposite. The prominent peak at 1022 cm^{-1} is assigned to the C−O−C of the β-1,4 glycosidic linkages between the sugar units of CMC. There is a reduction in the intensity of this peak in CAlFeC, and a much bigger reduction in CAlFeC-F, possibly due to surface coverage and also due to masking by fluoride. However, it has been shown that when the C−O−C links are vibrationally excited, all other atoms in the rings attached by that linkage are affected; hence, this peak cannot be assigned to the glycosidic link alone.[29] In the presence of an acidic solution of ferric chloride, some cellulose chains undergo hydrolysis and oxidation, leading to shorter oligosaccharide chains and gluconic acid.[30] This reaction is probably responsible for the cleavage of some C−O−C linkages in the cellulose chains and hence the lowering of intensity.

Raman spectra (Figure 3B) revealed the characteristic CMC features with few additional peaks due to the iron and aluminum oxyhydroxides in the composite. The broad peak between 300 and 500 cm^{-1} is due to the C−C−C, C−O−C, and C−C−O ring deformation of the glucopyranose rings. This peak became more prominent in CAlFeC and CAlFeC-F as it overlaps with the −OH vibration peaks of metal oxyhydroxides.[31] The Al−O characteristic peaks also appear in this region.[31] The peak at 729 cm^{-1} that appears in the nanocomposite is attributed to Fe−O stretching[23] but could be in combination with the γ vibration of OH groups of boehmite that also occurs at 730 cm^{-1}. The peak at 931 cm^{-1}, redshifted to 983 cm^{-1} in the composite, is assigned to COO^- deformation, whose intensity reduced in CAlFeC and CAlFeC-F as a result of strong metal−carboxylate group interaction highlighted in earlier IR data. The peak at 1115 cm^{-1} is attributed to C−O−C glycosidic stretch, with reduced intensities in CAlFeC and CAlFeC-F, possibly caused by restrictions to the vibrations of these groups as a result of confinement and masking in the composite matrix. The $-CH_2-$ twisting, wagging, and deformation peaks between 1200 and 1500 cm^{-1} become less prominent in the composite, which gives further evidence of a strong and complex interaction between CMC and other components of CAlFeC and adsorption of fluoride. Adsorption of fluoride did not significantly change the CAlFeC structure, implying physical adsorption rather than chemical transformation.

BET surface area for the as-prepared nanocomposite (before fluoride uptake) was obtained as 134.3 m^2/g. This high surface area is responsible for the excellent fluoride uptake capacity of CAlFeC. The average pore diameter of 74.259 Å was recorded, higher than what has been reported from similar materials.[13] This reveals the existence of mesopores in the material, which can be penetrated by free fluoride ions with an ionic radius of 1.47 Å. One may note that the surface area of best-performing materials is generally in this range and not very large.[11,13] The adsorbent recorded a pore volume of 0.298620 cm^3/g.

The XPS survey spectra of CAlFeC and CAlFeC-F are shown in Figure 4Aa,Ab, respectively. Deconvoluted peaks due to S 2p, Al 2p, Fe 2p, O 1s, C 1s, and F 1s are represented in Figure 4B−G, before (a) and after (b) adsorption of fluoride.

https://doi.org/10.1021/acssuschemeng.1c03272
ACS Sustainable Chem. Eng. 2021, 9, 12788−12799

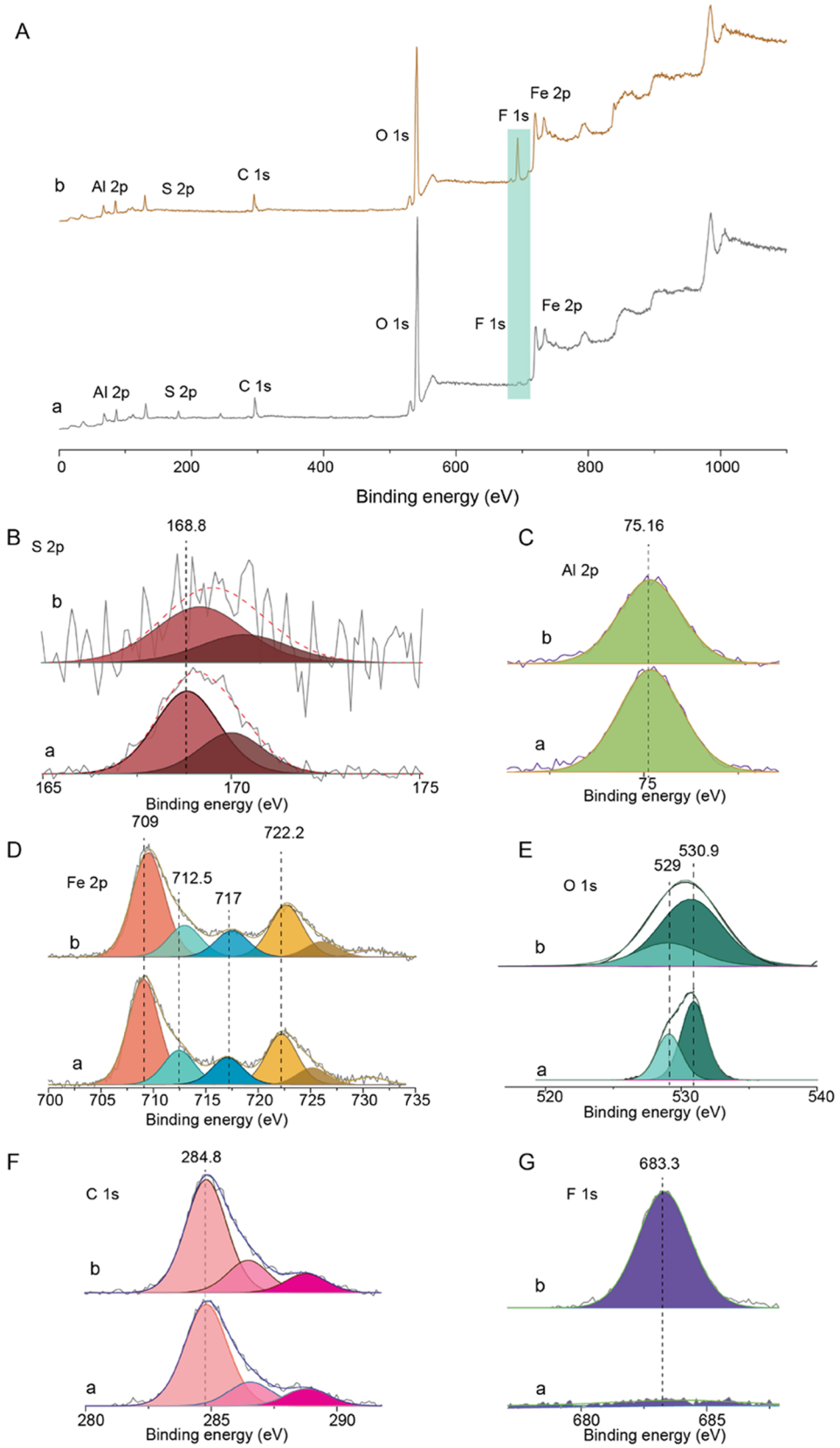

Figure 4. XPS features of CAlFeC: (A) survey spectra before (a) and after (b) fluoride adsorption; (B−G) XPS characteristics of the different elemental constituents of CAlFeC before (a) and after (b) fluoride uptake in each case.

The XPS spectrum of C 1s shows a characteristic peak at 284.8 eV for CAlFeC, which did not change after its interaction with fluoride. This is consistent with the observation by Mukherjee et al.[32] The peaks at 286.5 and 288.7 eV denote the presence of hydroxyl C−OH and carboxyl (C═O) bonds in the composite, which originate from

https://doi.org/10.1021/acssuschemeng.1c03272
ACS Sustainable Chem. Eng. 2021, 9, 12788−12799

CMC.[32] The XPS peaks corresponding to F 1s appeared at 683.3 eV in CAlFeC-F but were absent in CAlFeC. This confirms the fluoride adsorption onto CAlFeC. The peak due to Al 2p appeared at its characteristic position at 75.2 eV and did not show any significant shift upon fluoride adsorption. The O 1s peak was very prominent at 530.9 eV, which did not show a change in its position after adsorption (Figure 4E). The peak due to Fe 2p appeared at 709.0 eV in CAlFeC but redshifted to 709.5 eV in CAlFeC-F. This points to the change in the bonding environment of Fe, possibly the exchange of −OH for F^- at the iron centers, leading to their increased stabilization owing to the chemisorption of fluoride. The S 2p peak is also significantly shifted from 168.8 to 169.2 eV. Although the bonding nature of sulfate in the nanocomposite is not fully understood, this result suggests its participation in fluoride binding. Figure 4 shows that except for Fe 2p and S 2p, most peak positions remained largely unchanged after fluoride adsorption, suggesting that a combination of physisorption and chemisorption contribute to fluoride binding, in addition to ion exchange and electrostatic surface interactions.[33]

Direct shear stress measurement was essential to evaluate the strength of the adsorbent. Dry and wet samples of the material were separately mounted in a shear box, and normal stress of 50, 100, and 150 kPa were applied, respectively, and the horizontal shear displacement was measured, as shown in Figure S2A. Figure S2B shows the Mohr−Coulomb failure envelopes for the dry and wet materials. The calculated internal angle of friction (φ) shown were 58.7 and 54.3° for the dry and wet materials, respectively, depicting a hard material comparable to dense gravel sand, a feature that is highly desirable for adsorbent-based water purifiers.[34]

Effect of Adsorbent Dose, pH, Counterion, and Cycle Study. The extent of fluoride removal increased with an increase in the sorbent dose to a saturation point at about 1 g/L (Figure S6A). This was taken as the sorbent dose for further experiments. At this adsorbent dose and initial fluoride concentrations <20 mg/L, the number of adsorption sites available was sufficient to lower fluoride concentrations to the permissible limit.

Change in pH of the medium affects not only the speciation of fluoride in solution but also the protonation state and thus the surface charge density of the adsorbent. At a relatively low pH, the adsorbent surface acquires a net positive charge as a result of the protonation of surface groups, as shown in eq 1.

$$\equiv MOH + H^+ \rightarrow \equiv \overset{+}{M}OH_2 \quad (1)$$

This favors fluoride adsorption owing to electrostatic attraction and displacement of H_2O from the sites. However, when the pH is lower than 4, fluoride exists in a protonated form as HF, and the loss of negative charge lowers its uptake by the adsorbent.[22] From Figure S6B, we see that CAlFeC effectively adsorbs fluoride within a relatively wide pH range (4−9), consistent with other studies on similar materials.[32] Increase in pH beyond 9 lowered its fluoride uptake capacity. This is due to a negative charge imparted on the adsorbent surface at a pH higher than the pH_{pzc}, thereby repelling fluoride ions, consistent with other reports on similar materials.[3] Reduced fluoride adsorption at higher pH can also be attributed to competition for the adsorption sites with excess hydroxide ions.[22]

The effect of counterions, commonly present in environmental water, on the defluoridation capacity of CAlFeC was tested. It was observed that Cl^-, NO_3^-, SO_4^{2-}, Mg^{2+}, Ca^{2+}, Na^+, and K^+ did not significantly affect the fluoride uptake capacity of the adsorbent. However, the presence of CO_3^{2-}, HCO_3^-, PO_4^{3-}, and SiO_3^{2-} in contaminated water reduced the effectiveness of the adsorbent in the order $PO_4^{3-} > SiO_3^{2-} > CO_3^{2-} > HCO_3^- > SO_4^{2-}$ (Figure S6C). Fortunately, the levels of phosphate in environmental water are usually low. The bulky and highly charged orthophosphate anion is thought to be preferentially adsorbed to the cationic surface groups or blocks them, excluding fluoride. This is consistent with the research findings of another study, which found a similar trend of interference by coexisting ions.[35]

To regenerate an adsorbent sustainably, the eluent should have a quick desorbing ability, be affordable, and should not damage the adsorbent surface.[17] We, therefore, used NaOH and avoided acidic eluents that could easily react with metallic oxides in CAlFeC. The regeneration efficiency of the materials is shown in Figure S6D. When the spent adsorbent from the first cycle was washed with 2 mol/L NaOH, it retained 64% effective capacity even after the 4th cycle. The adsorbent can be regenerated and reused up to four times, hence reducing the cost of treated water. A higher concentration of NaOH was found to be a more effective regenerant.

Adsorption Isotherms. To gain an insight into the mechanism of adsorption, 100 mg of the adsorbent was contacted with 100 mL of varied initial fluoride concentrations (ranging from 3.2 to 202 mg/L) and stirred at 200 rpm in an orbital shaker for 24 h. The equilibrium adsorption capacity is usually expressed as the extent of adsorption in milligram of adsorbate loaded per gram of adsorbent (q_e), and the adsorption efficiency is calculated from eqs S1 and S2. The data obtained, presented in Table 2, were fitted into the Langmuir, Freundlich, Temkin, and Dubinin-Radushkevich adsorption isotherm models.

Table 2. Effect of the Initial Fluoride Concentration on the Adsorption Capacity of CAlFeC

C_o (mg/L)	C_e (mg/L)	q_e (mg/L)	fluoride removal (%)
3.2	0.09	3.11	97.2
6.2	0.2	6	96.8
10.5	0.46	10.04	95.6
17.3	0.89	16.41	94.9
27.2	2.6	24.6	90.4
52.7	14.5	38.2	72.5
78.9	32	46.9	59.4
105	48.5	56.5	53.8
157	91	66	42
202	125	77	38.1

From Table 2, we see that at the adsorbent dose of 1 g/L used, water containing up to 20 mg/L of fluoride can be effectively treated to the acceptable level of 1.5 mg/L. When the fluoride concentration is higher than 20 mg/L, a higher dose of CAlFeC can be used to achieve the required fluoride concentration in treated water. The amount of fluoride adsorbed (q_e) generally increased when higher initial fluoride concentrations were used, indicating the abundance of adsorption sites.

The Freundlich isotherm describes nonideal and reversible adsorption, usually physisorption, on heterogeneous adsorbent

https://doi.org/10.1021/acssuschemeng.1c03272
ACS Sustainable Chem. Eng. 2021, 9, 12788−12799

Table 3. Comparison of CAlFeC with Other Similar Adsorbents

adsorbent	solvent(s) used in synthesis	maximum synthesis temperature (°C)	optimum pH of use	adsorption capacity, q_{max} (mg/g)	ref
Al_2O_3-Fe_3O_4-expanded graphite	acetic acid, vitriol	450	2−10	2.19	35
chitosan-based Ti−Al binary metal oxide	acetic acid, hydrochloric acid	425	3−10	2.22	37
magnesium-iron-aluminum trimetal composite	water	600	3−9	92.85	38
cellulose nanofiber-polyaniline-templated ferrihydrite nanocomposite	aniline	room temperature	3−4	50.8	13
La-doped Li−Al-layered double hydroxides supported by a polymeric anion exchanger	water, ethanol	70	4−9	75.7	8
Fe_3O_4/Al_2O_3 nanoparticle-coated polyurethane foams	methanol, petroleum ether	100	2−6	43.47	16
chitosan-reinforced Zr_xAl_{1-x} OOH nanocomposites			3−10.5	9.44	17
cellulosic FeOOH/AlOOH composite	water	room temperature	4−9	75.2	this study

surfaces. This empirical model can be applied to multilayer adsorption, with a nonuniform distribution of heat of adsorption and affinities over the heterogeneous surface.[36] The linear form of Freundlich isotherm is given in eq S3 in the SI. Fitting our data to this model (Figure S7B) gave linear regression, $R^2 = 0.9603$. The slope ranging between 0 and 1 is a measure of adsorption intensity or surface heterogeneity, becoming more heterogeneous as its value reaches closer to zero. A value below 1 indicates chemisorption, while $1/n > 1$ depicts cooperative adsorption.[36] We obtained a slope of 0.4 and $n = 2.5$, implying a fairly heterogeneous adsorbent surface and favorable adsorption.[6] The linear form of Langmuir isotherm is given in eq S4 in the SI. This model assumes equivalent adsorption sites on a uniform sorbent surface and no interaction or transmigration of adsorbed particles in a monolayer surface coverage.[36] Our adsorption data fitted best to the Langmuir isotherm (Figure S7A), with $R^2 = 0.9729$, and with an impressive maximum adsorption capacity, $q_{max} = 75.2$ mg/g. Such a high value of q_{max} has hardly been attained by other reports of fluoride adsorption.

Many similar adsorbents reported in other studies are only effective at low pH, or are less effective at neutral pH, or are difficult to separate from treated water. Besides, many of the reported synthetic protocols utilize aggressive chemicals, solvents, and temperatures. These problems are effectively solved in the present study. From Table 3, CAlFeC compares favorably with other related adsorbents in ease of synthesis, performance, and optimum pH range.

This, however, is not surprising, given the high porosity and surface area of CAlFeC, and hence the availability of adsorption sites. This implied that fluoride was largely chemisorbed in a monolayer on equivalent sites on the sorbent surface. This is consistent with the proposed mechanism of fluoride interaction with a similar adsorbent studied by Barathi et al.[33] in which a combination of ion exchange, Coulombic attraction, and hydrogen bonding is believed to be responsible for fluoride adsorption. An essential feature of the Langmuir isotherm is the separation factor R_L, which is calculated from eq S5 in the SI. The R_L value indicates the adsorption to be either unfavorable ($R_L > 1$), favorable ($0 < R_L < 1$), or irreversible ($R_L = 0$). In this work, $0 < R_L < 1$, indicates favorable adsorption. The Temkin isotherm model is presented in eq S6. It was initially used to describe the adsorption of hydrogen onto platinum electrodes within acidic solutions.[36] Its derivation assumes a uniform distribution of binding energies of the adsorbate. This model assumes that the heat of adsorption of all molecules in the layer would decrease linearly rather than logarithmically with coverage. Our data agreed fairly with this model, with $R^2 = 0.9537$ (Figure S7C).

The Dubinin-Radushkevich isotherm model is usually used to describe the adsorption mechanisms involving heterogeneous surfaces with Gaussian energy distribution. It is represented as eq S7 in which the parameter ε is obtained from eq S8 in the SI. The Dubinin-Radushkevich isotherm model is temperature-dependent, and when adsorption data at different temperatures are fitted, all suitable data lie on a characteristic curve. The model has often successfully fitted high and intermediate adsorbate concentrations; however, our data did not fit very well ($R^2 = 0.79$), as shown in Figure S7D.

Adsorption Kinetics. To investigate adsorption kinetics, the effect of contact time on fluoride uptake was studied. Fluoride solution (100 mL, 10.4 mg/L) was shaken with 100 mg of the sorbent. About 5 mL of the solution was withdrawn at different time intervals and tested for residual fluoride. Figure S8A shows that up to 80% of the fluoride was removed within the first 3 min, and equilibrium was attained within the 30 min of contact, indicating fast adsorption kinetics. This is essential as clean water can be obtained within a few min of treatment with the adsorbent. In all other experiments, a contact time of 120 min was used to ensure reaching the equilibrium concentration. Kinetic data were fitted into pseudo-first-order, pseudo-second-order, and intraparticle diffusion models.

The Lagergren pseudo-first-order model is given by the eq S9 in the SI.[39,40] CAlFeC adsorption data did not fit very well into this model, with $R^2 = 0.917$ (Figure S8C). Ho and McKay[41] developed the pseudo-second-order kinetic model based on the assumption that the rate-limiting step is chemical adsorption involving valence forces through sharing or exchange of electrons between sorbent and sorbate. The pseudo-second-order model is given by the eq S10 in the SI. Fluoride adsorption onto CAlFeC fitted best into this model with linear regression, $R^2 = 0.9999$ (Figure S8B). This is also in agreement with the fact that fluoride adsorption onto CAlFeC also obeys the Langmuir isotherm, hence giving evidence for the predominance of chemisorption. In this case, we suggest that the exchange of fluoride ions for surface hydroxide of AlOOH and FeOOH is as shown in the proposed mechanism illustrated in eq 2 and Figure 5.

https://doi.org/10.1021/acssuschemeng.1c03272
ACS Sustainable Chem. Eng. 2021, 9, 12788−12799

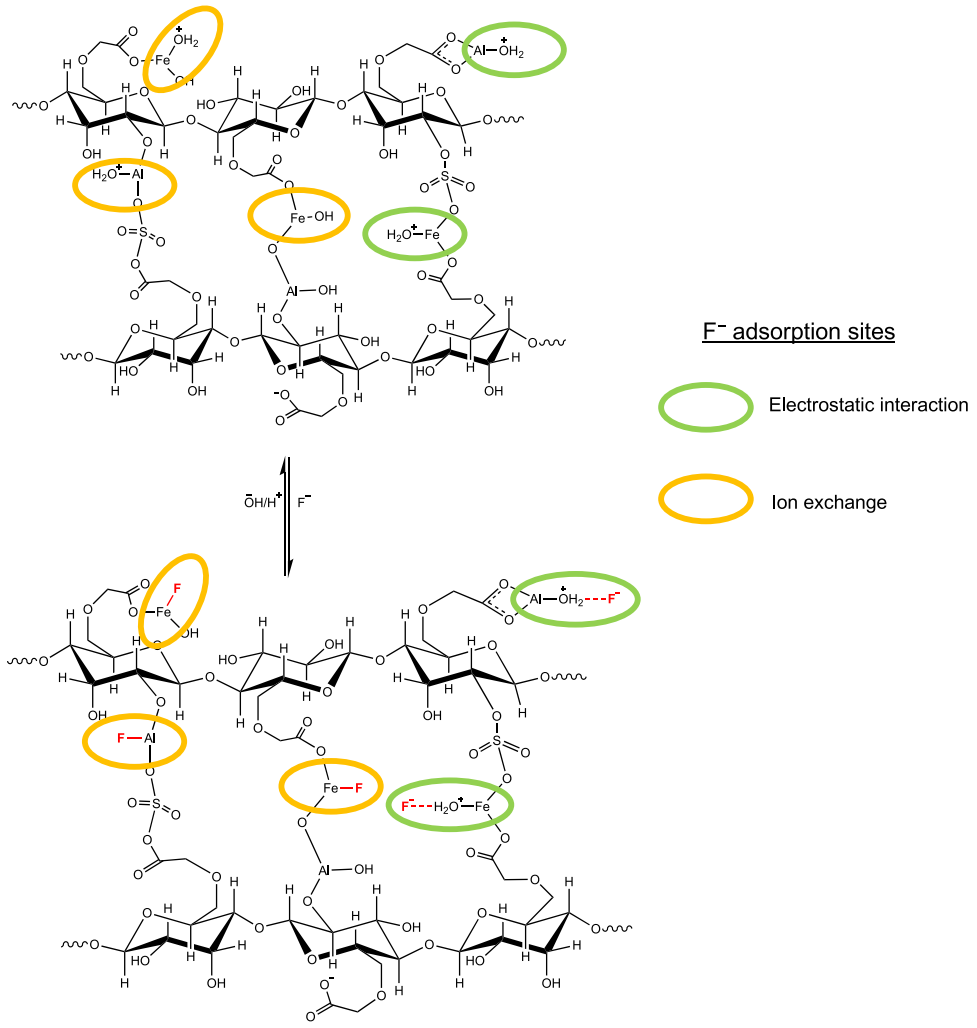

Figure 5. Proposed structure of CAlFeC and the suggested mechanism of fluoride adsorption. The metal centers shown here represent the oxyhydroxides.

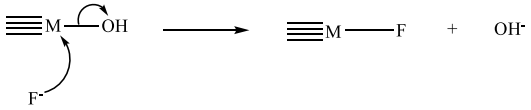

(2)

Other related studies have proposed a similar mechanism of fluoride adsorption.[20,33]

Ionic interaction with protonated surface groups such as $\equiv M - \overset{+}{O}H_2 - \cdots\cdots\cdots {}^{-}F$ is believed to be the other mechanisms of fluoride adsorption onto CAlFeC; moreover, protonated OH groups are good leaving groups that can be easily replaced by F^-. According to the Weber-Morris intraparticle diffusion kinetic model, in many adsorption cases, solute uptake varies almost proportionally with $t^{1/2}$ instead of t (where t is the contact time), as shown in eq S11[42] in the SI. The contribution of intraparticle diffusion in the transfer of adsorbate from the bulk of the solution into the porous solid structure cannot be ignored. This is often the rate-determining step when adsorption occurs in a rapidly stirred batch reactor.[43] Despite its contribution to the overall fluoride uptake, our experimental data fitted fairly to this model, with $R^2 = 0.9067$ (Figure S8D).

Leaching Experiment for TOC, Fe, and Al. The extent of leaching of total organic carbon (TOC), aluminum, and iron from the adsorbent into the treated water was evaluated. TOC was measured in the water before and after contact with CAlFeC using a TOC analyzer (Shimadzu TOC-V_{CPH}). The values of TOC were below the US-EPA permissible limit of 4 mg/L (Figure S5C); hence, there was no significant risk of formation of toxic organics even if chlorine disinfection was applied to the treated water. Leaching of iron and aluminum was determined using ICPMS (PerkinElmer NexION 300X). Ultrapure water before and after contact with the adsorbent was prepared in 5% nitric acid, and iron and aluminum were measured in a precalibrated ICPMS. The leaching protocol followed the US-EPA method 1311. The amount of iron was found to be below the US-EPA and WHO limits for drinking water, in the range of 64−140 μg/L, within the acceptable limit of 300 μg/L. Aluminum levels in purified water ranged from 26 to 120 μg/L in the experiments done with different particle sizes. All samples contained aluminum levels lower than the guideline value of 200 μg/L. These results indicate the inorganic components (metal oxyhydroxides) are mostly confined in the polymer cages, not easily leached, yet accessible to provide safe and clean drinking water upon removing fluoride.

Cartridge Experiment. A cartridge setup illustrated in Figure S5A was used to test the field applicability of CAlFeC to remove fluoride from water. Field water, with characteristics

https://doi.org/10.1021/acssuschemeng.1c03272
ACS Sustainable Chem. Eng. 2021, 9, 12788−12799

given in Table S1, was spiked with fluoride to 10.4 mg/L and passed through a cartridge packed with 21.7 g of CAlFeC of particle size 212 μm with the flow rate maintained at 10 mL/min. Figure S5B shows the changes in fluoride levels and pH of purified water after passing through the CAlFeC cartridge. It was found that about 20 liters of water contaminated with 10 mg/L of fluoride can be treated to less than 1.5 mg/L (WHO limit). Upon passing through CAlFeC, the pH of the water was slightly lowered from 8.0 to about 6.8, initially (Figure S5B), still within the normal pH range of 6.5−8.5 for potable water. This slight reduction in pH can be corrected by passing it through a second cartridge in series packed with a calculated amount of lime.

Sustainability Metrics. The sustainability of synthesis and utilization of CAlFeC was evaluated using sustainability indices and greenness parameters. These are the indicators of environment-conscious approaches to chemical reactions and manufacturing processes.[44−46] These indices were calculated using standard equations given in the SI, eqs S12−S16, and a summary of the results is shown in Table 4.

Table 4. Sustainability Metrics for the Synthesis and Use of CAlFeC

sl. no.	parameter	value
1	mass intensity (kg/kg)	5.68
2	water intensity (kg/kg)	36.67
3	reaction mass efficiency (%)	17.6
4	energy intensity (kW·h/kg)	2.0
5	*E* factor	0.124

Raw Materials. The major raw materials used were CMC, which was obtained from renewable plant materials, and the aluminum and iron salts used were nontoxic. The alkali used was neutralized during coprecipitation of an acidic solution of Al^{3+} and Fe^{3+}. The only solvent used was water, which is mostly reused and is easily recyclable. All raw materials are readily available and affordable.

Mass Intensity. Mass intensity is a measure of the total mass of materials used to produce a specified mass of product. Materials include reactants, reagents, and catalysts. Ideally, Mass intensity equals unity when no waste is produced and all materials are incorporated into the product. Mass intensity was determined from eq S12 and was found to be 5.68 kg/kg. This value could be improved by minimizing the loss of product during the filtration and washing process. Water intensity was estimated from eq S13 in the SI and was found to be 36.67 kg/kg, a relatively high figure, but comparable to the findings from other similar studies.[13,32] The water (over 95%) was used for washing the material, and this can be recycled and reused. A significantly large amount of water was used to wash the material before drying, and this spent water can be stored and used in the next several rounds of preliminary washing before it is recycled.

Reaction Mass Efficiency. Reaction mass efficiency was determined from eq S14, and a value of 17.6% was obtained. From our calculations, about 5 L of water (used mainly to wash the composite) is required to form 300 g of adsorbent, which can give about 300 L of purified water. The whole process is, therefore, water positive. Regeneration and reuse of adsorbent can significantly improve these figures.

Energy Intensity. Using eq S15, it was found that about 2 kW·h/kg of electricity was required for stirring, suction filtration, and oven-drying. Electricity cost could be reduced by scaling up the quantity of material synthesized and by utilizing sunshine to dry the material.

Resulting Emissions. The synthesis of CAlFeC does not produce any harmful solvents, fumes, or byproducts. Spent water used in washing has high TDS but can be recycled and reused. The *E* factor (environmental factor) was estimated from eq S16 and was found to be 0.124, an indication of a negligible amount of waste products during synthesis. An *E* factor close to the ideal value of zero signifies the optimal utilization of reagents and minimization of waste products.

Toxicity Potential. CMC is a nontoxic food-grade substance. $Al_2(SO_4)_3$ and $FeCl_3$ have low acute toxicity, and NaOH is corrosive.[47] They are nonflammable and stable at room temperature. Simple precautionary safety measures have to be taken during the synthesis of CAlFeC.

Disposal of Waste. The fluoride-loaded adsorbent can be regenerated and reused 3−4 times by treatment with a strong alkali. The spent adsorbent can be safely disposed of in leach-free landfills.

Affordability. This fluoride removal technology can provide fluoride-free water at a cost of about $3.3/kL of safe drinking water. This is comparable to the cost of an adsorbent synthesized in a related study[13] but reasonably more affordable compared to membrane technologies such as reverse osmosis.

CONCLUSIONS

The synthesis of an environmentally friendly, highly effective adsorbent for the removal of fluoride from water is presented in this report. Readily available and low-cost reagents were used to synthesize the adsorbent in an aqueous medium at room temperature. The synthesis protocol was optimized to ensure reduced cost, robustness, effectiveness, and ease of use. From several studies, the adsorbent was found to be a hard, porous, and largely amorphous solid but became semicrystalline upon electron beam irradiation. The adsorbent was applicable in a pH range of 4−9. Regeneration is possible by treatment with sodium hydroxide, and this would give up to four reusable cycles. It is effective for fluoride removal even in the presence of other ions commonly present in environmental waters, although PO_4^{3-} and SiO_3^{2-} ions significantly reduced its effectiveness. It was observed that no significant leaching of the adsorbent components (Al, Fe, and TOC) into treated water took place and the adsorbate-laden material met the leaching characteristics prescribed by the US-EPA. The material exhibited fast adsorption kinetics, following the pseudo-second-order model, with over 80% of fluoride removal happening within 3 min of contact. The approach presented confirms the possibility of creating sustainable absorbent materials with enhanced capacity by nanostructuring, using multiple components.

Isotherm studies showed that adsorption of fluoride follows the Langmuir adsorption model, largely as chemisorption through ion exchange and Coulombic attraction on charged groups. About 22 g of the adsorbent could effectively treat up to 20 L of water contaminated with 10 mg/L F^-. On evaluation of the sustainability and greenness of synthesis and use, the process was found to be water, energy, and atom efficient, with the only toxic waste being the spent adsorbent that can be safely disposed of in landfills. From estimation, the cost per liter of purified water is expected to be low, enabling its applicability in poor rural communities affected by excess fluoride in drinking water.

https://doi.org/10.1021/acssuschemeng.1c03272
ACS Sustainable Chem. Eng. 2021, 9, 12788−12799

■ ASSOCIATED CONTENT

Supporting Information

The Supporting Information is available free of charge at https://pubs.acs.org/doi/10.1021/acssuschemeng.1c03272.

Equations used in the main text; graphs showing the effect of incorporating different cations and anions into CAlFeC structure on its F^- uptake capacity; images showing stable and unstable adsorbent in contact with water; mechanical stability (hardness) of the adsorbent in dry and wet conditions; TEM-EDS and SEM-EDS elemental maps of CAlFeC before and after F^- adsorption; cartridge setup and results of leaching experiment; and adsorption isotherms and kinetics graphs (PDF)

■ AUTHOR INFORMATION

Corresponding Author

Thalappil Pradeep − *DST Unit of Nanoscience (DST UNS) and Thematic Unit of Excellence (TUE), Department of Chemistry, Indian Institute of Technology Madras, Chennai 600 036, India;* orcid.org/0000-0003-3174-534X; Email: pradeep@iitm.ac.in

Authors

Moses Egor − *Busitema University, 236 Tororo, Uganda; Mbarara University of Science and Technology, 1410 Mbarara, Uganda; DST Unit of Nanoscience (DST UNS) and Thematic Unit of Excellence (TUE), Department of Chemistry, Indian Institute of Technology Madras, Chennai 600 036, India*

Avula Anil Kumar − *DST Unit of Nanoscience (DST UNS) and Thematic Unit of Excellence (TUE), Department of Chemistry, Indian Institute of Technology Madras, Chennai 600 036, India;* orcid.org/0000-0001-6878-8736

Tripti Ahuja − *DST Unit of Nanoscience (DST UNS) and Thematic Unit of Excellence (TUE), Department of Chemistry, Indian Institute of Technology Madras, Chennai 600 036, India*

Sritama Mukherjee − *DST Unit of Nanoscience (DST UNS) and Thematic Unit of Excellence (TUE), Department of Chemistry, Indian Institute of Technology Madras, Chennai 600 036, India*

Amrita Chakraborty − *DST Unit of Nanoscience (DST UNS) and Thematic Unit of Excellence (TUE), Department of Chemistry, Indian Institute of Technology Madras, Chennai 600 036, India*

Chennu Sudhakar − *DST Unit of Nanoscience (DST UNS) and Thematic Unit of Excellence (TUE), Department of Chemistry, Indian Institute of Technology Madras, Chennai 600 036, India*

Pillalamarri Srikrishnarka − *DST Unit of Nanoscience (DST UNS) and Thematic Unit of Excellence (TUE), Department of Chemistry, Indian Institute of Technology Madras, Chennai 600 036, India;* orcid.org/0000-0001-5187-6879

Sandeep Bose − *DST Unit of Nanoscience (DST UNS) and Thematic Unit of Excellence (TUE), Department of Chemistry, Indian Institute of Technology Madras, Chennai 600 036, India*

Swathy Jakka Ravindran − *DST Unit of Nanoscience (DST UNS) and Thematic Unit of Excellence (TUE), Department of Chemistry, Indian Institute of Technology Madras, Chennai 600 036, India;* orcid.org/0000-0002-7882-7871

Complete contact information is available at: https://pubs.acs.org/10.1021/acssuschemeng.1c03272

Author Contributions

‖M.E. and A.A.K. contributed equally to this work.

Notes

The authors declare no competing financial interest.

■ ACKNOWLEDGMENTS

The authors thank Sugi Shivan for making FTIR measurements, Biswajit Modal for HRTEM-EDS, and Manu Santhanam for his help in conducting direct shear stress analysis. The authors are grateful to the technicians of the Department of Chemistry, IIT Madras, for helping to carry out PXRD and BET analyses. The authors thank Ramesh Kumar for his help in setting up the cartridge experiment. For their help in TOC measurements, the authors wish to thank Ligy Philip and Narasamma of the Department of Civil Engineering, IIT Madras. Finally, M.E. is grateful to all members of the Pradeep Research Group for their help with experimental work and interpretation. The authors thank IIT Madras and the Department of Science and Technology, Government of India, for supporting our research program on nanomaterials. M.E. is a student of Mbarara University of Science and Technology and was a research fellow at IIT Madras during this work.

■ REFERENCES

(1) Nagar, A.; Pradeep, T. Clean Water through Nanotechnology: Needs, Gaps, and Fulfillment. *ACS Nano* **2020**, *14*, 6420−6435.

(2) Raghav, S.; Kumar, D. Adsorption Equilibrium, Kinetics, and Thermodynamic Studies of Fluoride Adsorbed by Tetrametallic Oxide Adsorbent. *J. Chem. Eng. Data* **2018**, *63*, 1682−1697.

(3) Wan, Z.; Chen, W.; Liu, C.; Liu, Y.; Dong, C. Preparation and Characterization of Gamma-AlOOH @CS Magnetic Nanoparticle as a Novel Adsorbent for Removing Fluoride from Drinking Water. *J. Colloid Interface Sci.* **2015**, *443*, 115−124.

(4) Gai, W.-Z.; Zhang, S.-H.; Yang, Y.; Zhang, X.; Deng, Z.-Y. Separation of Excess Fluoride from Water Using Amorphous and Crystalline AlOOH Adsorbents. *ACS Omega* **2021**, *6*, 16488−16497.

(5) Carpenter, A. W.; deLannoy, C.-F.; Wiesner, M. R. Cellulose Nanomaterials in Water Treatment Technologies. *Environ. Sci. Technol.* **2015**, *49*, 5277−5287.

(6) Viswanathan, N.; Sundaram, C. S.; Meenakshi, S. Sorption Behaviour of Fluoride on Carboxylated Cross-Linked Chitosan Beads. *Colloids Surf., B* **2009**, *68*, 48−54.

(7) Gericke, M.; Trygg, J.; Fardim, P. Functional Cellulose Beads: Preparation, Characterization, and Applications. *Chem. Rev.* **2013**, *113*, 4812−4836.

(8) Cai, J.; Zhang, Y.; Qian, Y.; Shan, C.; Pan, B. Enhanced Defluoridation Using Novel Millisphere Nanocomposite of La-Doped Li-Al Layered Double Hydroxides Supported by Polymeric Anion Exchanger. *Sci. Rep.* **2018**, *8*, No. 11741.

(9) Jing, C.; Cui, J.; Huang, Y.; Li, A. Fabrication, Characterization, and Application of a Composite Adsorbent for Simultaneous Removal of Arsenic and Fluoride. *ACS Appl. Mater. Interfaces* **2012**, *4*, 714−720.

(10) Zhang, J.; Kong, Y.; Yang, Y.; Chen, N.; Feng, C.; Huang, X.; Yu, C. Fast Capture of Fluoride by Anion-Exchange Zirconium−Graphene Hybrid Adsorbent. *Langmuir* **2019**, *35*, 6861−6869.

(11) Kumar, A. A.; Som, A.; Longo, P.; Sudhakar, C.; Bhuin, R. G.; Gupta, S. Sen.; Anshup; Sankar, M. U.; Chaudhary, A.; Kumar, R.; Pradeep, T. Confined Metastable 2-Line Ferrihydrite for Affordable

Point-of-Use Arsenic-Free Drinking Water. *Adv. Mater.* **2017**, *29*, No. 1604260.
(12) Sankar, M. U.; Aigal, S.; Maliyekkal, S. M.; Chaudhary, A.; Anshup; Kumar, A. A.; Chaudhari, K.; Pradeep, T. Biopolymer-Reinforced Synthetic Granular Nanocomposites for Affordable Point-of-Use Water Purification. *Proc. Natl. Acad. Sci. USA* **2013**, *110*, 8459−8464.
(13) Mukherjee, S.; Ramireddy, H.; Baidya, A.; Amala, A. K.; Sudhakar, C.; Mondal, B.; Philip, L.; Pradeep, T. Nanocellulose-Reinforced Organo-Inorganic Nanocomposite for Synergistic and Affordable Defluoridation of Water and an Evaluation of Its Sustainability Metrics. *ACS Sustainable Chem. Eng.* **2020**, *8*, 139−147.
(14) Abouzeid, R. E.; Khiari, R.; El-Wakil, N.; Dufresne, A. Current State and New Trends in the Use of Cellulose Nanomaterials for Wastewater Treatment. *Biomacromolecules* **2019**, *20*, 573−597.
(15) Hussain, Z.; Daosheng, L.; Xi, L.; Jianxiong, K. Defluoridation by a Mg−Al−La Triple-Metal Hydrous Oxide: Synthesis, Sorption, Characterization and Emphasis on the Neutral pH of Treated Water. *RSC Adv.* **2015**, *5*, 43906−43916.
(16) Kumari, S.; Khan, S. Defluoridation Technology for Drinking Water and Tea by Green Synthesized Fe_3O_4/Al_2O_3 Nanoparticles Coated Polyurethane Foams for Rural Communities. *Sci. Rep.* **2017**, *7*, No. 8070.
(17) Prabhu, S. M.; Sasaki, K. Fabrication of Chitosan-Reinforced ZrxAl1-XOOH Nanocomposites and Their Arsenite and Fluoride Depollution Densities from Single/Binary Systems. *ChemistrySelect* **2017**, *2*, 6375−6387.
(18) WHO. *Fluorides and Oral Health*; WHO: Geneva, 1994; Vol. *846*.
(19) Chen, H.; Yan, M.; Yang, X.; Chen, Z.; Wang, G.; Schmidt-Vogt, D.; Xu, Y.; Xu, J. Spatial Distribution and Temporal Variation of High Fluoride Contents in Groundwater and Prevalence of Fluorosis in Humans in Yuanmou County, Southwest China. *J. Hazard. Mater.* **2012**, *235*−*236*, 201−209.
(20) Rathore, V. K.; Mondal, P. Competitive Adsorption of Arsenic and Fluoride onto Economically Prepared Aluminum Oxide/Hydroxide Nanoparticles: Multicomponent Isotherms and Spent Adsorbent Management. *Ind. Eng. Chem. Res.* **2017**, *56*, 8081−8094.
(21) Klemm, D.; Philipp, B.; Heinze, T.; Heinze, U.; Wagenknecht, W. *Comprehensive Cellulose Chemistry: Functionalization of Cellulose*; Wiley-VCH Verlag GmbH: Weinheim, 1998; *Vol. 2*.
(22) Chen, Y.; Zhang, Q.; Chen, L.; Bai, H.; Li, L. Basic Aluminum Sulfate@graphene Hydrogel Composites: Preparation and Application for Removal of Fluoride. *J. Mater. Chem. A* **2013**, *1*, No. 13101.
(23) Hanesch, M. Raman Spectroscopy of Iron Oxides and (Oxy)Hydroxides at Low Laser Power and Possible Applications in Environmental Magnetic Studies. *Geophys. J. Int.* **2009**, *177*, 941−948.
(24) Saalfeld, H.; Wedde, M. Refinement of the Crystal Structure of Gibbsite, $Al(OH)_3$. *Z. Krist.* **1974**, *139*, 129−135.
(25) Wolska, E. The Structure of Hydrohematite. *Z. Krist.: Cryst. Mater.* **1981**, *154*, 69−76.
(26) Arami, H.; Mazloumi, M.; Khalifehzadeh, R.; Sadrnezhaad, S. K. Electron Beam-Induced "Nanocalcination" of Boehmite Nanostrips to Mesoporous α-Alumina Phase. *J. Am. Ceram. Soc.* **2007**, *90*, 3311−3313.
(27) Colthup, N. B.; Daly, L. H.; Wiberley, S. E. *Introduction to Infrared and Raman Spectroscopy*, 3rd ed.; Academic Press, Inc.: Sandiego, 1990.
(28) Dudev, T.; Lim, C. Monodentate versus Bidentate Carboxylate Binding in Magnesium and Calcium Proteins: What Are the Basic Principles? *J. Phys. Chem. B* **2004**, *108*, 4546−4557.
(29) Makarem, M.; Lee, C. M.; Kafle, K.; Huang, S.; Chae, I.; Yang, H.; Kubicki, J. D.; Kim, S. H. Probing Cellulose Structures with Vibrational Spectroscopy. *Cellulose* **2019**, *26*, 35−79.
(30) Zhang, H.; Li, N.; Pan, X.; Wu, S.; Xie, J. Direct Transformation of Cellulose to Gluconic Acid in a Concentrated Iron(III) Chloride Solution under Mild Conditions. ACS Sustain. *Chem. Eng.* **2017**, *5*, 4066−4072.
(31) Ruan, H. D.; Frost, R. L.; Kloprogge, J. T. Comparison of Raman Spectra in Characterizing Gibbsite, Bayerite, Diaspore and Boehmite. *J. Raman Spectrosc.* **2001**, *32*, 745−750.
(32) Mukherjee, S.; Kumar, A. A.; Sudhakar, C.; Kumar, R.; Ahuja, T.; Mondal, B.; Srikrishnarka, P.; Philip, L.; Pradeep, T. Sustainable and Affordable Composites Built Using Microstructures Performing Better than Nanostructures for Arsenic Removal. *ACS Sustainable Chem. Eng.* **2019**, *7*, 3222−3233.
(33) Barathi, M.; Krishna Kumar, A. S.; Kumar, C. U.; Rajesh, N. Graphene Oxide−Aluminium Oxyhydroxide Interaction and Its Application for the Effective Adsorption of Fluoride. *RSC Adv.* **2014**, *4*, 53711−53721.
(34) David, E. Mechanical Strength and Reliability of the Porous Materials Used as Adsorbents/ Catalysts and the New Development Trends. *Arch. Mater. Sci. Eng.* **2015**, *73*, 5−17.
(35) Xu, C.; Li, J.; He, F.; Cui, Y.; Huang, C.; Jin, H.; Hou, S. Al_2O_3−Fe_3O_4−Expanded Graphite Nano-Sandwich Structure for Fluoride Removal from Aqueous Solution. *RSC Adv.* **2016**, *6*, 97376−97384.
(36) Foo, K. Y. Y.; Hameed, B. H. H. Insights into the Modeling of Adsorption Isotherm Systems. *Chem. Eng. J.* **2010**, *156*, 2−10.
(37) Thakre, D.; Jagtap, S.; Sakhare, N.; Labhsetwar, N.; Meshram, S.; Rayalu, S. Chitosan Based Mesoporous Ti-Al Binary Metal Oxide Supported Beads for Defluoridation of Water. *Chem. Eng. J.* **2010**, *158*, 315−324.
(38) Zhao, W.; Chen, Y.; Zhang, W.; Wang, J.; Hu, C.; He, W. Synthesis, Performance, and Mechanism of Magnesium-Iron-Aluminum Trimetal Composite as an Adsorbent for Fluoride Removal in Water Treatment. *Can. J. Chem. Eng.* **2016**, *94*, 2289−2297.
(39) Qiu, H.; Lv, L.; Pan, B.; Zhang, Q.; Zhang, W.; Zhang, Q. Critical Review in Adsorption Kinetic Models. *J. Zhejiang Univ., Sci., A* **2009**, *10*, 716−724.
(40) Yuh-Shan, H. Citation Review of Lagergren Kinetic Rate Equation on Adsorption Reactions. *Scientometrics* **2004**, *59*, 171−177.
(41) Ho, Y. S.; McKay, G. The Kinetics of Sorption of Divalent Metal Ions onto Sphagnum Moss Peat. *Water Res.* **2000**, *34*, 735−742.
(42) Alkan, M.; Demirbaş, Ö.; Doğan, M. Adsorption Kinetics and Thermodynamics of an Anionic Dye onto Sepiolite. *Microporous Mesoporous Mater.* **2007**, *101*, 388−396.
(43) Kannan, N.; Sundaram, M. M. Kinetics and Mechanism of Removal of Methylene Blue by Adsorption on Various Carbons—a Comparative Study. *Dyes Pigments* **2001**, *51*, 25.
(44) Sheldon, R. A. Metrics of Green Chemistry and Sustainability: Past, Present, and Future. *ACS Sustainable Chem. Eng.* **2018**, *6*, 32−48.
(45) Makeower, J. The Tenth Annual State of Green Business, *Phoenix*, 2017.
(46) Cohen, S.; Bose, S.; Guo, D.; Miller, A.; Berger, O.; DeFrancia, K.; Filiatraut, B.; Qiu, W.; Loman, M.; Zhang, C. *The Growth of Sustainability Metrics; Sustainability Metrics White Paper Series,*1 of 3, 2014.
(47) NCBI. Aluminum Sulfate, CID=24850 https://pubchem.ncbi.nlm.nih.gov/compound/Aluminum-sulfate (accessedJuly 4, 2020).

https://doi.org/10.1021/acssuschemeng.1c03272
ACS Sustainable Chem. Eng. 2021, 9, 12788−12799